

# Emergence of global receptive fields capturing multipartite quantum correlations

Oleg M. Sotnikov,<sup>1,2</sup> Ilya A. Iakovlev,<sup>1,2</sup> Evgeniy O. Kiktenko,<sup>2,3</sup>  
Mikhail I. Katsnelson,<sup>4</sup> Aleksey K. Fedorov,<sup>2,3</sup> and Vladimir V. Mazurenko<sup>1,2</sup>

<sup>1</sup>*Theoretical Physics and Applied Mathematics Department,  
Ural Federal University, Ekaterinburg 620002, Russia*

<sup>2</sup>*Russian Quantum Center, Skolkovo, Moscow 121205, Russia*

<sup>3</sup>*National University of Science and Technology “MISIS”, Moscow 119049, Russia*

<sup>4</sup>*Institute for Molecules and Materials, Radboud University,  
Heyendaalseweg 135, 6525AJ, Nijmegen, Netherlands*

(Dated: August 26, 2024)

In quantum physics, even simple data with a well-defined structure at the wave function level can be characterized by extremely complex correlations between its constituent elements. The inherent non-locality of the quantum correlations generally prevents one from providing their simple and transparent interpretation, which also remains a challenging problem for advanced classical techniques that approximate quantum states with neural networks. Here we show that monitoring the neural network weight space while learning quantum statistics from measurements allows to develop physical intuition about complex multipartite patterns and thus helps to construct more effective classical representations of the wave functions. Particularly, we observe the formation of distinct global convolutional structures, receptive fields in the hidden layer of the Restricted Boltzmann Machine (RBM) within the neural quantum tomography of the highly-entangled Dicke states. On this basis we propose an exact two-parameter classical representation not only for a specific quantum wave function, but for the whole family of the  $N$ -qubit Dicke states of different entanglement. Our findings suggest a fresh look at constructing convolutional neural networks for processing data with non-local patterns and pave the way for developing exact learning-based representations of entangled quantum states.

## INTRODUCTION

Machine learning is among the most promising modern technologies, which has a vast impact on all areas of activities. Recognizing and classifying objects, translating languages, generating texts [1] and videos, creating images [2], playing games [3–5], predicting human lives [6] are only some examples of the tasks that can be solved with modern artificial neural networks. In scientific domain, neural networks accelerate search for novel materials [7], recognize different phases of matter [8], facilitate simulations of complex quantum systems [9, 10] with the number of particles inaccessible to standard methods such as exact diagonalization, help to discover quantum-error-correction strategies against noise [11] and solve many other problems. It also suggests a new scientific paradigm which can be applied far beyond “exact sciences”, for example, in the evolutionary biology [12].

Such a success of neural networks in different areas is mainly related to the possibility of capturing spatial, temporal and other correlations in input data. In this respect the concept of the receptive fields (RF) first introduced in neuroscience [13–15] for describing spatial behavior of animals holds significant importance in developing convolutional neural networks (CNN) [16, 17]. RF assumes that the input image contains highly correlated repeating local features. To capture them each unit from the first hidden layer of CNN can interact with only a portion of the input neurons (sparse connectivity) and such hidden neurons related to different parts of the image are then combined in a feature map where they

share the same weights. This makes CNN invariant to shift transformations (translations) and provides its success in solving different tasks [18–20]. Remarkably, it has been found that CNN can be used in quantum physics to approximate quantum wave functions defined on regular lattices [21]. Here, introducing rotations, mirror symmetries and other transformations [22] into consideration positively affects the solution of complex problems in condensed matter physics [23].

The use of the RF concept that the input is characterized by some topology is not limited to CNN, it can be realized for other neural network architectures. For instance, the account of the regular lattice symmetries when simulating quantum spin Hamiltonians with Restricted Boltzmann Machines allows to reduce the total number of variational parameters and considerably improve the accuracy of the modeling [9]. Interestingly, the account of symmetries leads to formation of the receptive fields capturing quantum correlations in one- and two-dimensional magnetic systems.

Another level of modeling RFs suggests detecting their emergence when the neural network learns from scratch without imposing symmetries on the weights. As the bright example of this one can consider the RBM trained with Ising model configurations in Ref. [24] to reproduce the corresponding probabilities. Importantly, the shape of the resulting receptive fields was shown to reflect the magnetic correlations in the system in question. In general case preparing of the input data can play a decisive role in observing RFs. For instance, in Ref. [25] analyzing the weight space of a simple dense neural network trained

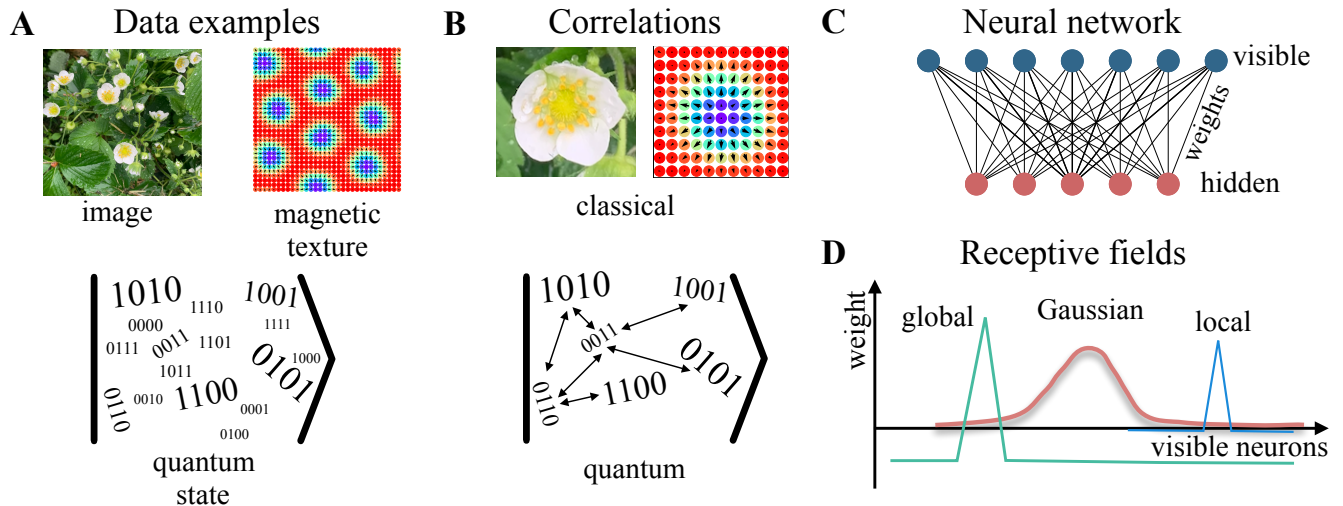


FIG. 1. From data through correlations to receptive fields. (A) A few examples of data that can be explored with neural networks. (B) Fragments cropped from (A) from which one can extract information about small-scale spatial correlations. In the quantum case the correlations defined by a parent Hamiltonian are schematically denoted with arrow lines. (C) An example of neural network with highlighted couplings between visible neurons and a hidden neuron that can host a receptive field capturing correlations in a system. (D) Comparison of the weight-space profiles of the receptive fields obtained in this work for quantum states (global RF) and those introduced in previous studies (local and Gaussian RFs).

by using the data with non-Gaussian high-order correlated structures, the authors have revealed and characterized receptive fields that resemble the filters of the convolutional neural networks. In quantum domain, the examples of the receptive field emergence have been found when solving the ground state problem for quantum XXZ model Hamiltonian with RBM representation of the wave function [26]. Here the receptive fields can be classified as local, since each hidden unit has non-zero interaction with only one visible neuron. Similar local RF were analytically derived within the neural quantum state tomography [27] for some notable wave functions (see also Refs. [28, 29]). Typically, the size of the receptive fields spontaneously developed in hidden layers of neural networks is much smaller than the working space monitored by visible neurons. This reflects the finite length of the correlations in the input data and makes the situation beyond these limits practically unexplored.

In our paper, we demonstrate that a distinct kind of global receptive fields is developed when neural network is trained to reproduce the state probabilities of a quantum system defined on the complete graph and characterized by multipartite correlations. For that, by using RBM we perform a neural quantum state tomography of the Dicke states [30] of different complexity. A remarkable property of thus found global RFs is that they emerge as the entanglement of the target quantum state increases. The profile of our RFs differs from those reported in the previous works. Each hidden unit has a maximal positive coupling with a single visible neuron and nearly constant negative coupling with the rest ones (Fig.1).

Undoubtedly, the crucial impact of learning RFs is the possibility to create and explore advanced neural network architectures, which allows reducing the total number of the network parameters and obtain more accurate solutions of a problem, as previously demonstrated in the case of the CNN. In our study we show that the learned global RFs can be used as filters for the restricted Boltzmann machine in the task of reconstructing quantum states of different entanglement. In this case a single compact RBM with the same number of the hidden and visible units allows exactly reconstructing the whole family of Dicke states from simple to complex ones.

## I. RESULTS

### A. Permutation structure and correlations of the Dicke states

We start by analyzing the properties of the real-valued non-negative wave functions that belong to the Dicke state family,

$$|\Psi_N^D\rangle = \frac{1}{\sqrt{C_D^N}} \sum_j P_j (|0\rangle^{\otimes N-D} \otimes |1\rangle^{\otimes D}), \quad (1)$$

where  $N$  is the number of qubits,  $D$  is the parameter that controls the number of “1”s in each basis function contributing to the particular quantum state and the sum goes over all possible permutations of qubits, denoted by  $P_j$ . As a simple example one can consider  $N = 4$  for which the wave functions with  $D = 1$  and  $D = 2$  are

given by

$$\frac{|0001\rangle + |0010\rangle + |0100\rangle + |1000\rangle}{2},$$

and

$$\frac{|0011\rangle + |0110\rangle + |1100\rangle + |1001\rangle + |1010\rangle + |0101\rangle}{\sqrt{6}},$$

respectively. The former wave function has a simple structure, each contributing basis state can be obtained by translating another one, which corresponds to cyclic permutation of the element 0001 ( $0001 \rightarrow 0010 \rightarrow 0100 \rightarrow 1000$ ). It is not the case for  $|\Psi_4^2\rangle$  which has a more complicated permutation structure. Here reproducing the whole wave function requires considering two disjoint cyclic permutations for initial elements 0011 and 0101,  $0011 \rightarrow 0110 \rightarrow 1100 \rightarrow 1001$  and  $0101 \rightarrow 1010$ . For larger  $N$  the number of such disjoint permutations will increase as the Dicke index,  $D$  becomes larger and reach the maximum at  $D = \frac{N}{2}$ . Thus, from the perspective of constructing a convolutional neural network, exploring Dicke states with  $D > 1$  will require a more complicated block of feature maps than that for  $D = 1$ .

The difference in structure of the permutations used for constructing  $|\Psi_N^D\rangle$  with different  $D$  parameters is intimately related to variance of quantum correlations of these functions. The previous consideration [31] of the quantum correlations on the level of the density matrices with relative entropy has demonstrated that the Dicke states with  $D = \frac{N}{2}$  display correlations at any order of a coarse grained partition of the system in question, which evidences a complex multipartite structure of these wave functions. From the perspective of applying a quantum state neural network approach in which one is to approximate unknown probability distribution for the basis functions of a target state, it is instructive to analyze the classical averages that are the correlation functions between qubits. For that we calculate the Ursell functions [32] (connected correlations) up to fourth order for spin operators,  $\hat{\sigma}_i^\alpha$ , where  $i$  is the site index and  $\alpha$  stands for the projection  $x, y$  or  $z$ . In our case we concentrate on the first order local correlations,  $\Gamma_i^\alpha$  and non-local correlation functions of higher orders,  $\Gamma_{ij}^{\alpha\beta}$ ,  $\Gamma_{ijk}^{\alpha\beta\gamma}$  and  $\Gamma_{ijkl}^{\alpha\beta\gamma\delta}$  ( $i \neq j \neq k \neq l$ ). The corresponding expressions for these correlation functions are given in Appendix C (Fig. 7).

Fig. 2 gives the calculated Ursell correlation functions for  $D = 1, 4$  and  $8$  of the 16-qubit system. In all the cases the connected correlations are invariant with respect to the choice of the qubit indexes and sensitive to the particular combination of the spin projections. In the lowest order we obtain non-zero  $\Gamma_i^z$  only with  $D = 1$  and  $4$ . In turn, the two-spin  $\Gamma$  reveal ferromagnetic correlations that amplify as the Dicke index increases. This can be explained by considering the Dicke wave functions as eigenstates of the Lipkin-Meshkov-Glick model [33–35] which is characterized by the ferromagnetic in-plane couplings defined on the complete  $N$ -node graph.

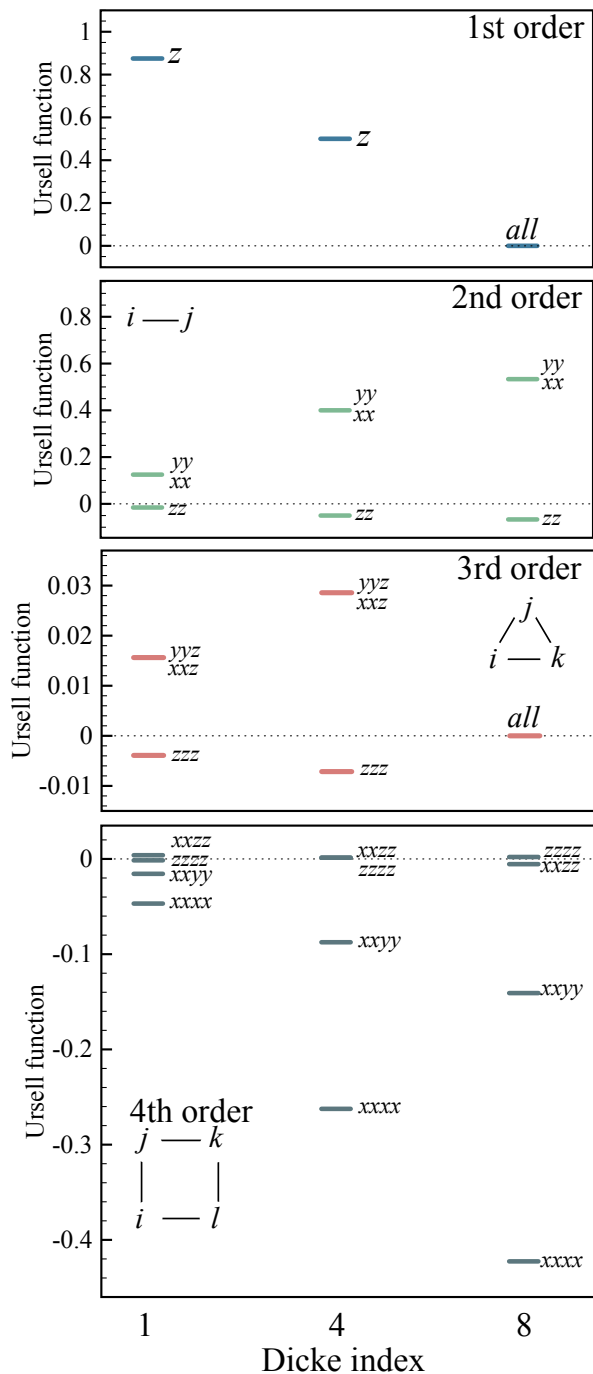


FIG. 2. Ursell functions up to 4th order that show the correlations structure of the 16-qubit Dicke states. The labels such as  $xxzz$  denote spin projection indexes of the calculated correlation functions. In the case of the 3rd and 4th order Ursell functions the correlation levels are multiply degenerate and for presentation purposes each level is associated only with one of correlation functions. The complete correlation histograms are presented in Appendix C. *all* stands for the cases when all the correlation functions are zero.

As one would expect, increasing the order of the  $\Gamma$

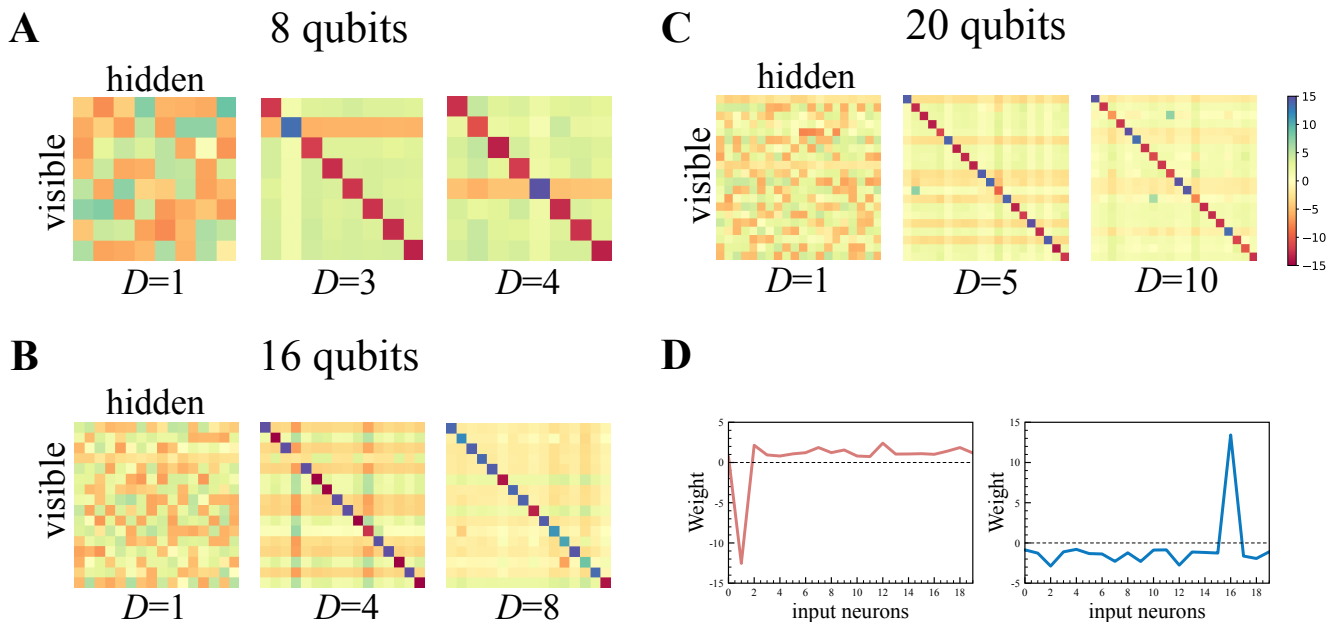


FIG. 3. Emergence of receptive fields in the weight space of the trained RBMs. (A-C) The neural quantum state tomography results obtained for the 8-, 16- and 20-qubit Dicke wave functions with different  $D$  index. In all the cases the number of visible and hidden neurons is the same. The overlaps of the constructed RBMs with exact wave functions are 0.997 (A,  $D = 1$ ), 0.935 (A,  $D = 3$ ), 0.928 (A,  $D = 4$ ), 0.994 (B,  $D = 1$ ), 0.88 (B,  $D = 4$ ), 0.709 (B,  $D = 8$ ), 0.991 (C,  $D = 1$ ), 0.728 (C,  $D = 5$ ) and 0.605 (C,  $D = 10$ ). (D) Examples of the connectivity of two hidden neurons taken from the 20-qubit calculations with  $D=10$ . For all the presented examples the neural quantum state tomography procedure was performed with 10000 bitstring samples in the training set.

function leads to more diverse picture of correlations. At the same time, the values of the non-local  $\Gamma_{ijkl}^{\alpha\beta\gamma\delta}$  are not small, as their strength is of the same order of magnitude as those for the two-spin correlation functions. Moreover, increasing the index  $D$  clearly demonstrates enhancement of the 4th order  $\Gamma$  function, which is a remarkable feature of the Dicke states. This evidences that the correlation structure of  $|\Psi_N^D\rangle$  is substantially non-local and is characterized by high-order excitations. Thus, learning the Dicke states with tomography procedure involves tuning restricted Boltzmann machine in such a way that it can reproduce undamped classical spin correlations of all orders, which would equally mean reconstructing genuine multipartite quantum correlations previously discussed in Ref. [31].

### B. Learning correlations with global receptive fields

We are now in position to discuss the neural quantum state tomography for the Dicke states, Eq.1 and to show that the receptive fields capturing non-local correlations can be discovered within the training without imposing symmetries. In the tomography approach the target wave function is to be approximated with positive

neural quantum state

$$|\Psi_\lambda\rangle = \sum_{\mathbf{v}} \Psi_\lambda(\mathbf{v}) |\mathbf{v}\rangle. \quad (2)$$

Here, the amplitude  $\Psi_\lambda$  of a given basis state  $|\mathbf{v}\rangle$  is estimated with a neural network that is characterized by the set of weights,  $\lambda$  and takes the bitstring  $\mathbf{v} = \{v_1, \dots, v_N\}$  of the binary variables as the input. Generally, approximating quantum states can be fulfilled with using neural networks of different architectures including restricted Boltzmann machine [9, 10, 27, 36], convolution [21], feed forward [37], recurrent [38, 39] and transformer neural networks [40, 41].

Following the previous works devoted to neural quantum state tomography [27] of the Dicke wave functions, we employ RBM neural network as realized in the QuCumber package [42]. In this case the basis states are characterized by the amplitudes  $\Psi_\lambda(\mathbf{v}) = \sqrt{p_\lambda(\mathbf{v})}$  and the corresponding probabilities

$$p_\lambda(\mathbf{v}) = Z_\lambda^{-1} e^{\sum_{i=1}^N a_i v_i} \prod_{j=1}^M (1 + e^{b_j + \sum_{i=1}^N W_{ij} v_i}), \quad (3)$$

where  $N$  ( $M$ ) is the number of the visible (hidden) units,  $\lambda = \{\mathbf{a}, \mathbf{b}, \mathbf{W}\}$  denotes the parameters of the restricted Boltzmann machine and the partition function  $Z_\lambda$  ensures the normalization of  $p_\lambda$ .  $W_{ij}$  is the weight matrix between visible and hidden units and  $a_i$  ( $b_j$ ) is the

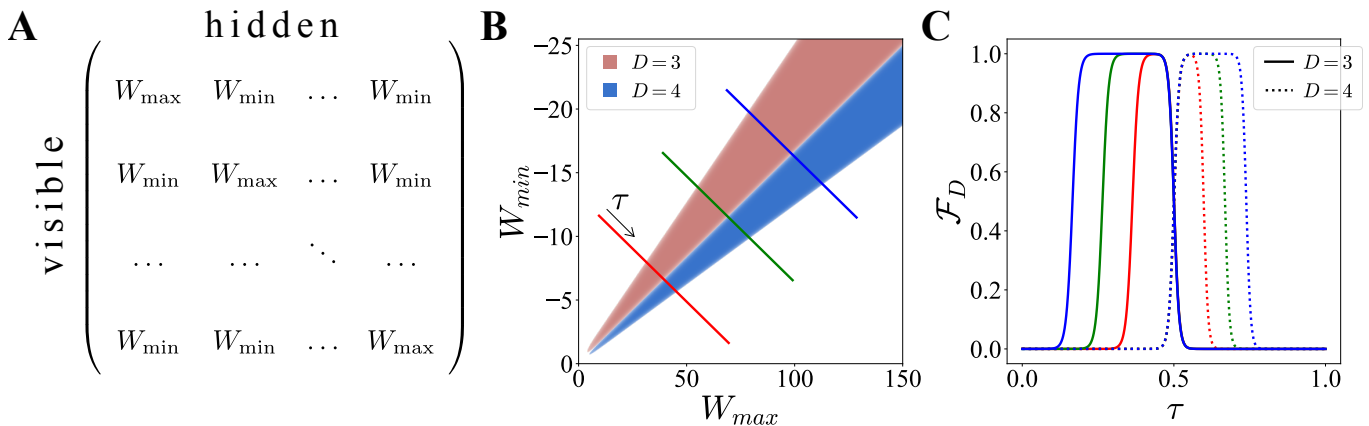


FIG. 4. Structural properties and phase diagram of the compact RBM we used to describe the 8-qubit Dicke family. (A) Weight matrix we used to simulate the Dicke states family with RBM. (B) Dicke states sectors in  $W_{\min}$ - $W_{\max}$  parameter space with  $D = 3$  and  $D = 4$  for NQS with  $N = 8$  visible neurons. Lines denote fidelity calculation paths. (C) Fidelity as function of  $\lambda$  defined along three different paths. Lines colors in (B) correspond to line colors in (C).

bias of the  $i$ th visible ( $j$ th hidden) neuron. The goal of the tomographic procedure is to optimize the network weights in such a way that the approximated wave function, Eq.3 has the largest overlap with the target wave function that is one of the Dicke states, Eq.1. For these purposes, one uses the Kullback-Leibler divergence [43] as the loss function. Importantly, the information about the target wave function is only represented in the form of finite sets of the bitstrings obtained from projective measurements. The comprehensive description of the neural quantum state tomography procedure we use can be found in Refs. [27, 42, 44].

Previously, the real-valued Dicke states with  $D = 1$  (known as the  $W$  state) for the systems of 20, 40 and 80 qubits were reconstructed with the neural quantum state tomography [27]. Since the  $|\Psi_N^1\rangle$  is the simplest wave function in the Dicke family and is characterized by the smallest entanglement, the RBM used for the tomography contains the same number of visible and hidden units. The reported overlap between the ideal  $W$  state and its RBM approximation for  $N = 20$  qubits is very high, 0.997. To our knowledge, the tomographic results for the other states with larger  $D$  that belong to the family have not been demonstrated. At the same time by increasing the Dicke index  $D$  from 1 to  $\frac{N}{2}$ , one increases the complexity of the quantum state as discussed in the previous section. In our work we focus on these highly-entangled states.

Fig. 3 visualizes the neural quantum state tomography results which are the elements of the weight matrices,  $W_{ij}$  between visible and hidden neurons of the RBMs we used to approximate different Dicke states for 8-, 16 and 20-qubit systems. The resulting weight matrices are square, since in all the cases the number of hidden and visible neurons is the same. One can see that for the simplest wave functions with  $D = 1$  the hidden units show random-like patterns of interactions with neurons from the visible layer. In this case absolute values of the

$W$  matrix elements do not exceed 9. In agreement with the results of Ref. 27 the target states with  $D = 1$  are reconstructed with high fidelity of 0.99 independent on the system size.

Remarkably, the solutions of the tomographic problem obtained for more entangled wave functions with  $D > 1$  reveal distinct patterns of the elements of the weight matrices. Each hidden unit is characterized by the receptive fields having non-zero weights with all the input neurons. There is a maximal (positive) or minimal (negative) interaction with the specific visible neuron, which indicates weight sharing and is an important feature of convolution [16]. Weak non-zero couplings to all other neurons from visible layer (Fig.3 D) reflect a distinct type of correlations of the input data. Thus, in the case of the RBMs approximating the Dicke states with large  $D$ , the whole weight space is uniformly covered with such global RFs.

The results presented in this section were obtained for 8-, 16- and 20-qubit systems by using the optimization procedure as described in Ref.[27] with the same number of input and hidden neurons. As one would expect, the increase of the Dicke index  $D$  leads to a considerable degradation of reconstructing the quantum states (Fig.3), and the number of the hidden units should be substantially increased so that the overlap is close to 90% (Appendix A). Below we show that when constructing RBM to approximate a Dicke wave function one can work around the hard problem of the neural quantum tomography by utilizing the architecture constructed with the revealed global receptive fields.

### C. A compact and exact RBM representation for all $N$ -qubit Dicke states with global RFs

Searching for exact classical neural network representations of complex entangled quantum states is one of the challenging tasks in modern science [45–47]. If possi-



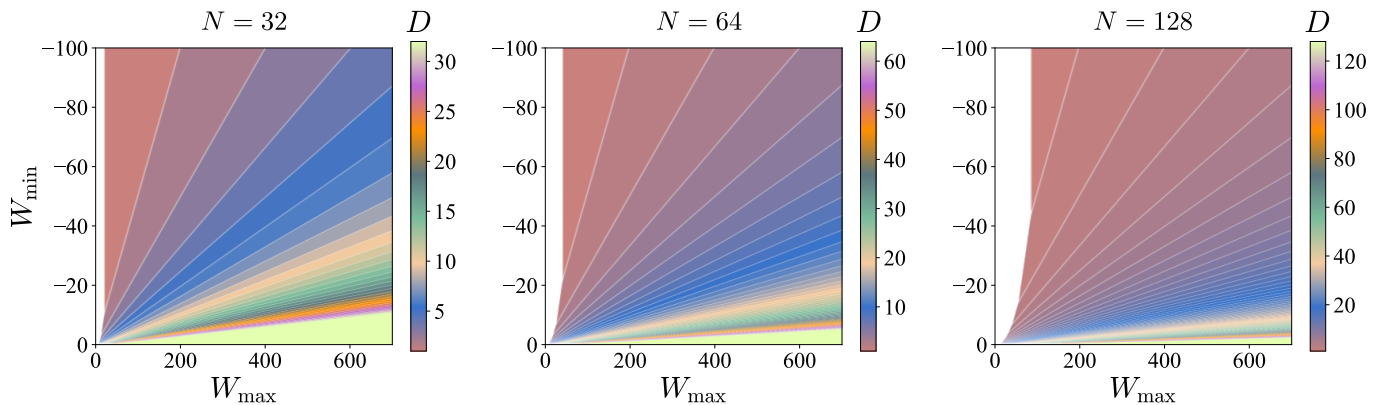


FIG. 5. Dicke states diagram for different system sizes obtained with classical RBM representation developed in this work. Colorbars denote value of the  $D$  parameter and white areas indicate superposition of different Dicke states such that fidelity of NQS with any of  $N$  Dicke states is not larger than 0.5.

ble, this avoids performing expensive training procedure and saves computer resources by compressing information about a wave function using the weights of a neural network. In this sense, the Dicke states are no exception. As shown in Ref.[27] the  $|\Psi_N^D\rangle$  wave function can be represented exactly with RBM, however, for that one should reserve single hidden unit for each pair of qubits in the system in question. This means the total number of parameters grows as  $N^2$  as the system size increases. The most compact representation of a  $N$ -qubit Dicke state with arbitrary  $D$  in terms of the number of hidden neurons so far has been reported in Ref.[48]. In this work the author has used a correlator product state approach to encode  $|\Psi_N^D\rangle$  and analytically showed that any Dicke wave function can be described with  $M = \lfloor \frac{N}{2} \rfloor$ . Here, we are going to demonstrate that by using global receptive fields one can develop exact and compact RBM representation for the whole Dicke wave functions family with  $M = N$ .

To imitate the Dicke states with RBM, we employ a non-sparse circular square weight matrix,  $W$  that is schematically presented in Fig.4 and is filled with only two real-valued parameters,  $W_{\min}$  and  $W_{\max}$ . Taking into account the structure of the discovered global receptive field, in our model RBM each hidden neuron has the  $W_{\max}$  interaction with one unique visible unit and the  $W_{\min}$  with other visible sites. Importantly, these weights are of different signs,  $W_{\min} < 0$  and  $W_{\max} > 0$ . Since  $M = N$ ,  $W$  is the square matrix and according to Ref.[26] our RBM can be classified as compact one. The biases for visible and hidden neurons are set to zero,  $\mathbf{a} = \mathbf{b} = 0$ . Constraining weight matrix structure in such a way makes the amplitudes of the basis states with the same number of "1"s to be the same. In other words, all the basis functions can be distinguished by the parameter  $d = \sum_i v_i$ . For the given  $W_{\min}$  and  $W_{\max}$  the basis functions,  $|\mathbf{v}\rangle$  that are characterized by the same  $d$  have

the same amplitude

$$\Psi_{\lambda}(d) = \frac{(1 + e^{W_{\max} + (d-1)W_{\min}})^{\frac{d}{2}} (1 + e^{dW_{\min}})^{\frac{N-d}{2}}}{\sqrt{Z_{\lambda}}}. \quad (4)$$

Thus, the RBM wave function of the system in question can be rewritten as

$$|\Psi_{\lambda}\rangle = \sum_{\mathbf{v}} \Psi_{\lambda}(d[\mathbf{v}]) |\mathbf{v}\rangle, \quad (5)$$

where  $d[\mathbf{v}] = \sum_i v_i$ .

To construct the  $W_{\min} - W_{\max}$  phase diagram that distinguishes the RBM states with respect to the Dicke wave functions with different indices  $D$ , the continuous parameter space is first discretized with a mesh. Then, for each point of the mesh the fidelities,  $\mathcal{F}_D$  between the neural quantum state  $|\Psi_{\lambda}\rangle$  and all the Dicke states are calculated. More specifically, one defines a set of fidelities  $\mathcal{F}_D = |\langle \Psi_N^D | \Psi_{\lambda} \rangle|^2$ , where  $0 \leq D \leq N$ . In general case, such fidelity calculations require determination of the normalization constant,  $Z_{\lambda}$  and summation over the whole basis states, which cannot be performed for large number of qubits  $N$ . Fortunately, the proposed architecture of the neural quantum state allows to directly estimate its fidelity with any Dicke state by means of the following expression:

$$\mathcal{F}_D = \left( 1 + \sum_{d \neq D} \frac{\tilde{p}_{\lambda}(d)}{\tilde{p}_{\lambda}(D)} \frac{(N-D)!D!}{(N-d)!d!} \right)^{-1} \quad (6)$$

Here,  $\tilde{p}_{\lambda}(d)$  are unnormalized RBM probabilities (Eq.3 without normalization constant) for basis functions with Dicke index  $d$ . In this way one can attribute a given point in weight parameter space  $\lambda = \{W_{\min}, W_{\max}\}$  to specific Dicke state or a composition of Dicke states.

Fig. 4 B gives an example where the neural networks with parameters denoted with red and blue colors are characterized by the 100% fidelity with the  $D = 3$  and

$D = 4$  Dicke states, respectively. Importantly, the narrow transition area (Fig. 4 C) between two sectors corresponds to a superposition of the aforementioned Dicke wave functions. To demonstrate the feasibility of our approach for representing entangled quantum states with global receptive fields in Fig. 5 we show the complete phase diagrams of the Dicke states for the systems with  $N = 32, 64$  and  $128$  qubits.

It is also possible to derive a condition on  $W_{\max} > 0$  and  $W_{\min} < 0$  that maximizes the fidelity for a given Dicke state. Consider the case, in which  $K$  of  $N$  visible neurons are active, and let us find the optimal configuration of hidden neurons that maximizes the system's energy. Enabling any hidden neuron that is not connected to  $K$  active visible neurons decreases the total energy by  $KW_{\min}$ , so these neurons are preferably inactive. At the same time, enabling  $K$  remaining hidden neurons causes a shift in energy of  $\Delta E = W_{\max} + (K - 1)W_{\min}$ . Given  $\Delta E > 0$ , the energy will be maximized by activating all  $K$  hidden neurons connected to  $K$  activated visible neurons. The total energy in this case is  $K\Delta E = KW_{\max} + K(K - 1)W_{\min}$ . The maximum over  $K$  is obtained when  $K = (1 - W_{\max}/W_{\min})/2$ . In this way, unit fidelity for  $|\Psi_N^D\rangle$  is achieved when

$$\frac{W_{\max}}{-W_{\min}} = 2D - 1 \quad (7)$$

and  $W_{\max}$  approaching infinity, which suppresses finite-temperature fluctuations. We observe that the RF-type symmetrical structure of the RBM weights “selects” states in the visible (and also the hidden) layers with a specific number of excitations. The high nonlocality of the weight matrix, shown in Fig. 4, manifests itself through a complex pattern of correlations among the resulting Dicke states, which is demonstrated in Fig. 2.

As soon as the RBM parameters are attributed to the particular Dicke state the corresponding entanglement entropy can be calculated analytically [49] for any bipartition. In the same spirit one can define genuine multipartite correlations for  $|\Psi_N^D\rangle$  [31].

## II. DISCUSSIONS AND PERSPECTIVES

Deep convolution networks with local receptive fields are known to be computationally inefficient for capturing large-scale correlations in data of different origin, which stimulates developing distinct types of the neural models such as non-local neural networks [50] and transformers [51]. Constructing non-local receptive fields to extend the capabilities of CNN and other architectures is problem specific and hard to do from scratch. However, our study devoted to approximation of the entangled Dicke wave functions shows that one can employ additional unsupervised learning tools such as quantum neural state tomography and, in this way, get basic information about optimal structure of the receptive fields within the learning procedure. Remarkably, based on our results con-

cerning the Dicke states such a learning does not have to be perfect.

As an interesting direction for future investigations we consider searching for receptive fields when performing neural quantum state tomography on the basis of simple and deep RBMs for wave functions characterized by different amount and structure of entanglement, for instance Greenberger–Horne–Zeilinger state, the tensor product of maximally entangled two-qubit states and others. In the same spirit, one can analyze the weight spaces of the trained RBM approximating ground states of quantum Hamiltonians on regular lattices, for instance one dimensional Ising model and Heisenberg Hamiltonian on the square lattice and others. In some cases neural network models of the aforementioned wave functions are known [26, 27, 45–48] and we expect to find receptive fields of different shapes and properties, which facilitates developing distinct compact classical representations for these quantum states through learning.

The development of the exact and compact classical neural network representations of quantum states with receptive field concept can be also perspective for more accurate estimation of different observables with sampling procedure [44] and derivation of the exact expressions for entanglement entropy [52], which eventually may facilitate establishing the connection between classical correlation functions and entanglement measures, which is an actual problem in the quantum information field that considers the entanglement as the physical resource to transfer information and perform complex computations [53, 54].

## ACKNOWLEDGEMENTS

The work of OMS, IAI, EOK, AKF and VVM was supported by the Russian Roadmap on Quantum Computing (Contract No. 868-1.3-15/15-2021, October 5, 2021). The work of EOK and AKF is supported by the Priority 2030 program at the “MISIS” University under the project K1-2022-027. The authors declare that this work has been published as a result of peer-to-peer scientific collaboration between researchers. The provided affiliations represent the actual addresses of the authors in agreement with their digital identifier (ORCID) and cannot be considered as a formal collaboration between Radboud University and the other aforementioned institutions.

### Appendix A: Neural quantum state tomography of the Dicke states

In this section we describe the details of the neural quantum state tomography whose results are presented in the main text. All the simulations presented in the main text were performed with the following parameters. We used 10 steps within the contrastive divergence procedure

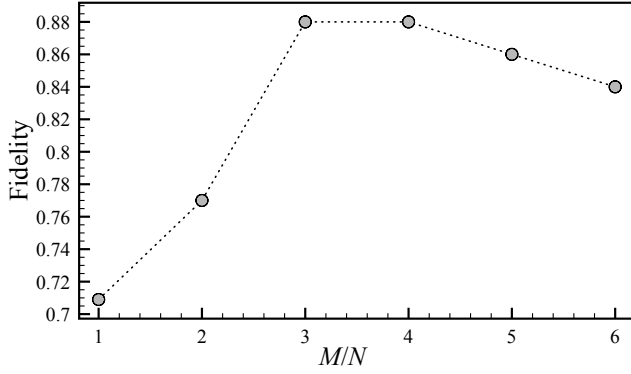


FIG. 6. Fidelity between ideal  $|\Psi_{16}^8\rangle$  Dicke wave function and its RBM approximations obtained within neural quantum state tomography for different number of the hidden neurons. In these numerical experiments the learning rate was taken to be 0.01.

and the learning rate was taken to be 0.1. The maximal number of the training epochs was set to 2000. However, in some calculations we observed the degradation of the results concerning fidelity with the target quantum state. That is why the neural network weights corresponding to the best fidelity have been selected for further analysis.

The results presented in Fig.3 in the main text were obtained with the same number of the hidden and visible neurons. Since the complexity of the quantum states enhances as the Dicke index increases we observe the degradation in reconstructing the target state as described in the main text. This problem can be solved by increasing the number of the hidden neurons and decreasing the learning rate. From Fig.6 plotted for the  $|\Psi_{16}^8\rangle$  state characterized by the largest entanglement it follows that the quality of the neural network approximation can be slightly improved by adding more hidden neurons, which likewise confirms the importance of the RF approach we develop in this work.

### Appendix B: Derivation of the fidelity expression

To derive Eq. (6) in the main text we start with relation between neural quantum state (2) and Dicke state (1):

$$|\Psi_\lambda\rangle = \sum_{d=0}^N \sqrt{p_\lambda(d) C_d^N} |\Psi_N^d\rangle \quad (\text{B1})$$

where  $p_\lambda(d)$  are normalized RBM probabilities:

$$p_\lambda(d) = Z_\lambda^{-1} \tilde{p}_\lambda(d) = \frac{\tilde{p}_\lambda(d)}{\sum_{i=0}^N \tilde{p}_\lambda(i) C_i^N} \quad (\text{B2})$$

Then, one can write the following expression for fidelity:

$$\mathcal{F}_D = |\langle \Psi_N^D | \Psi_\lambda \rangle|^2 = p_\lambda(D) C_D^N \quad (\text{B3})$$

Substitution of (B2) in (B3) gives equation (6) in the main text.

### Appendix C: Ursell functions

Below, we present the expressions for Ursell functions used to describe the classical correlations of the Dicke states

$$\Gamma_i^\alpha = \langle \hat{\sigma}_i^\alpha \rangle, \quad (\text{C1})$$

$$\Gamma_{ij}^{\alpha\beta} = \langle \hat{\sigma}_i^\alpha \hat{\sigma}_j^\beta \rangle - \langle \hat{\sigma}_i^\alpha \rangle \langle \hat{\sigma}_j^\beta \rangle, \quad (\text{C2})$$

$$\Gamma_{ijk}^{\alpha\beta\gamma} = \langle \hat{\sigma}_i^\alpha \hat{\sigma}_j^\beta \hat{\sigma}_k^\gamma \rangle - \langle \hat{\sigma}_i^\alpha \rangle \langle \hat{\sigma}_j^\beta \hat{\sigma}_k^\gamma \rangle - \langle \hat{\sigma}_j^\beta \rangle \langle \hat{\sigma}_i^\alpha \hat{\sigma}_k^\gamma \rangle - \langle \hat{\sigma}_k^\gamma \rangle \langle \hat{\sigma}_i^\alpha \hat{\sigma}_j^\beta \rangle + 2 \langle \hat{\sigma}_i^\alpha \rangle \langle \hat{\sigma}_j^\beta \rangle \langle \hat{\sigma}_k^\gamma \rangle, \quad (\text{C3})$$

and

$$\begin{aligned} \Gamma_{ijkl}^{\alpha\beta\gamma\delta} &= \langle \hat{\sigma}_i^\alpha \hat{\sigma}_j^\beta \hat{\sigma}_k^\gamma \hat{\sigma}_l^\delta \rangle - \langle \hat{\sigma}_i^\alpha \rangle \langle \hat{\sigma}_j^\beta \hat{\sigma}_k^\gamma \hat{\sigma}_l^\delta \rangle \\ &- \langle \hat{\sigma}_j^\beta \rangle \langle \hat{\sigma}_i^\alpha \hat{\sigma}_k^\gamma \hat{\sigma}_l^\delta \rangle - \langle \hat{\sigma}_k^\gamma \rangle \langle \hat{\sigma}_i^\alpha \hat{\sigma}_j^\beta \hat{\sigma}_l^\delta \rangle - \langle \hat{\sigma}_l^\delta \rangle \langle \hat{\sigma}_i^\alpha \hat{\sigma}_j^\beta \hat{\sigma}_k^\gamma \rangle \\ &- \langle \hat{\sigma}_i^\alpha \hat{\sigma}_j^\beta \rangle \langle \hat{\sigma}_k^\gamma \hat{\sigma}_l^\delta \rangle - \langle \hat{\sigma}_i^\alpha \hat{\sigma}_k^\gamma \rangle \langle \hat{\sigma}_j^\beta \hat{\sigma}_l^\delta \rangle - \langle \hat{\sigma}_i^\alpha \hat{\sigma}_l^\delta \rangle \langle \hat{\sigma}_j^\beta \hat{\sigma}_k^\gamma \rangle \\ &+ 2 \langle \hat{\sigma}_i^\alpha \hat{\sigma}_j^\beta \rangle \langle \hat{\sigma}_k^\gamma \rangle \langle \hat{\sigma}_l^\delta \rangle + 2 \langle \hat{\sigma}_i^\alpha \hat{\sigma}_k^\gamma \rangle \langle \hat{\sigma}_j^\beta \rangle \langle \hat{\sigma}_l^\delta \rangle \\ &+ 2 \langle \hat{\sigma}_i^\alpha \hat{\sigma}_l^\delta \rangle \langle \hat{\sigma}_j^\beta \rangle \langle \hat{\sigma}_k^\gamma \rangle + 2 \langle \hat{\sigma}_j^\beta \hat{\sigma}_k^\gamma \rangle \langle \hat{\sigma}_i^\alpha \rangle \langle \hat{\sigma}_l^\delta \rangle \\ &+ 2 \langle \hat{\sigma}_j^\beta \hat{\sigma}_l^\delta \rangle \langle \hat{\sigma}_i^\alpha \rangle \langle \hat{\sigma}_k^\gamma \rangle + 2 \langle \hat{\sigma}_k^\gamma \hat{\sigma}_l^\delta \rangle \langle \hat{\sigma}_i^\alpha \rangle \langle \hat{\sigma}_j^\beta \rangle \\ &- 6 \langle \hat{\sigma}_i^\alpha \rangle \langle \hat{\sigma}_j^\beta \rangle \langle \hat{\sigma}_k^\gamma \rangle \langle \hat{\sigma}_l^\delta \rangle. \quad (\text{C4}) \end{aligned}$$

Here  $\alpha$  ( $\beta$ ,  $\gamma$ ,  $\delta$ ) stands for spin projection of the Pauli matrix,  $\langle \dots \rangle = \langle \Psi_N^D | \dots | \Psi_N^D \rangle$  denotes the average calculated for the wave function  $|\Psi_N^D\rangle$ . Fig.7 gives the complete histograms of the non-zero Ursell functions of 3rd and 4th orders.

[1] OpenAI, GPT-4 Technical Report, arXiv:2303.08774  
[2] Anton Razzhigaev, Arseniy Shakhmatov, Anastasia Maltseva, Vladimir Arkhipkin, Igor Pavlov, Ilya Ryabov, Angelina Kuts, Alexander Panchenko, Andrey Kuznetsov, Denis Dimitrov, Kandinsky: an Improved Text-to-Image Synthesis with Image Prior and Latent

Diffusion, arXiv:2310.03502.  
[3] V. Mnih et al., Nature 518, 529 (2015).  
[4] D. Silver et al., Nature 529, 484 (2016).  
[5] N. Brown, T. Sandholm, Science 365, 885 (2019)  
[6] Germans Savcisen, Tina Eliassi-Rad, Lars Kai Hansen, Laust Hvas Mortensen, Lau Lilleholt, Anna Rogers, Ingo



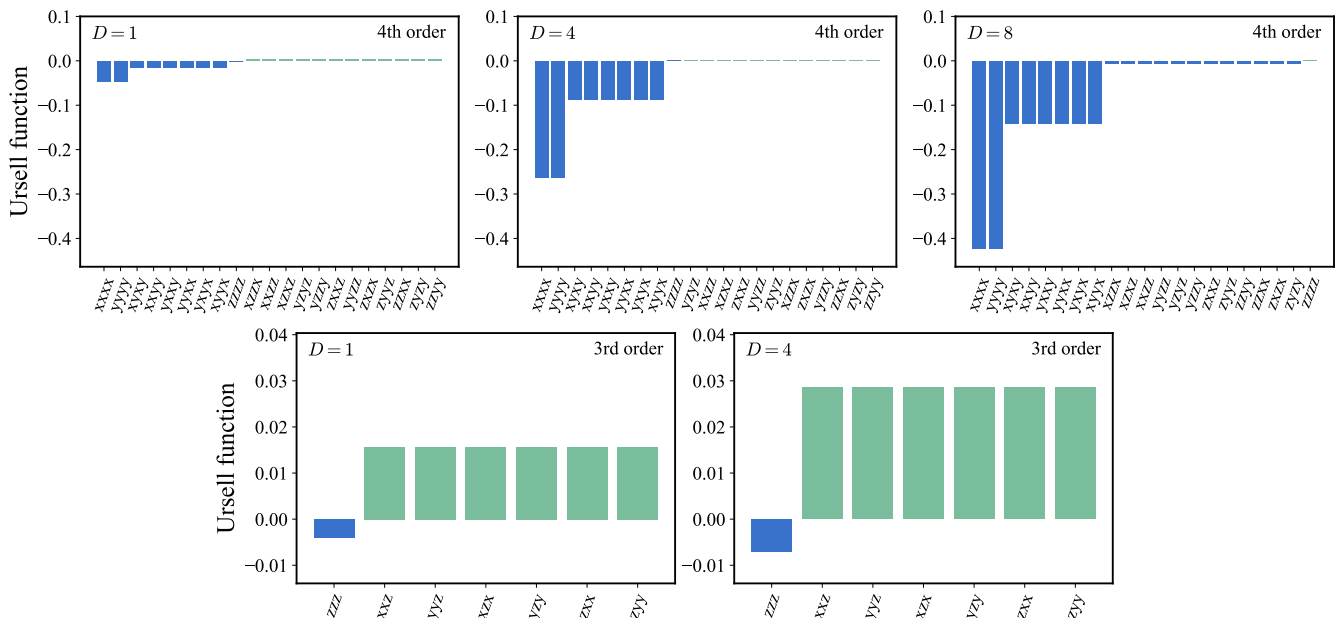


FIG. 7. Non-zero Ursell functions  $\Gamma$  for 16-site Dicke states with  $D = 1, 4, 8$ . The labels such as  $xxxx$  denote spin projection indexes of the calculated correlation functions.

- Zettler and Sune Lehmann, Using sequences of life-events to predict human lives, *Nature Computational Science* (2023).
- [7] Amil Merchant, Simon Batzner, Samuel S. Schoenholz, Muratahan Aykol, Gowoon Cheon and Ekin Dogus Cubuk, Scaling deep learning for materials discovery, *Nature* 624, 80 (2023)
- [8] Juan Carrasquilla and Roger G. Melko, Machine learning phases of matter, *Nature Physics* 13, 431 (2017)
- [9] G. Carleo, M. Troyer, Solving the quantum many-body problem with artificial neural networks, *Science* 355, 602 (2017)
- [10] Yusuke Nomura and Masatoshi Imada, Dirac-Type Nodal Spin Liquid Revealed by Refined Quantum Many-Body Solver Using Neural-Network Wave Function, Correlation Ratio, and Level Spectroscopy, *Phys. Rev. X* 11, 031034 (2021)
- [11] Thomas Fösel, Petru Tighineanu, Talitha Weiss, and Florian Marquardt, *Phys. Rev. X* 8, 031084 (2018)
- [12] V. Vanchurin, Y. I. Wolf, M. I. Katsnelson, and E. V. Koonin, Toward a theory of evolution as multilevel learning, *Proc. Natl. Acad. Sci. U.S.A.* **119**, e2120037119 (2022)
- [13] D.H. Hubel and T.N. Wiesel, Receptive fields, binocular interaction and functional architecture in the cat's visual cortex, *J. Physiol.* 160, 106 (1962)
- [14] John O'Keefe, Neil Burgess, Geometric determinants of the place fields hippocampal neurons, *Nature* 381, 425 (1996).
- [15] Roddy M. Grieves, Selim Jedidi-Ayoub, Karyna Mishchanchuk, Anyi Liu, Sophie Renaudineau and Kate J. Jeffery, The place-cell representation of volumetric space in rats, *Nat Commun* 11, 789 (2020).
- [16] Y. LeCun, L. Bottou, Y. Bengio, and P. Haffner, "Gradient-based learning applied to document recognition", *Proceedings of the IEEE*, vol. 86, no. 11, pp. 2278–2324, November 1998
- [17] M. Norouzi, M. Ranjbar, G. Mori, "Stacks of convolutional restricted Boltzmann machines for shift-invariant feature learning," in *Proceedings of the IEEE Conference on Computer Vision and Pattern Recognition*, 20 to 25 June 2009 (IEEE, 2009), pp. 2735–2742.
- [18] Izhar Wallach, Michael Dzamba, Abraham Heifets, AtomNet: A Deep Convolutional Neural Network for Bioactivity Prediction in Structure-based Drug Discovery, arXiv:1510.02855
- [19] Edward Grefenstette, Phil Blunsom, Nando de Freitas, Karl Moritz Hermann, A Deep Architecture for Semantic Parsing, arXiv:1404.7296
- [20] Ciresan, Dan; Meier, Ueli; Schmidhuber, Jürgen (June 2012). "Multi-column deep neural networks for image classification". *2012 IEEE Conference on Computer Vision and Pattern Recognition*. New York, NY: Institute of Electrical and Electronics Engineers (IEEE). pp. 3642–3649. arXiv:1202.2745
- [21] Kenny Choo, Titus Neupert, and Giuseppe Carleo, Two-dimensional frustrated  $J_1$ - $J_2$  model studied with neural network quantum states, *Phys. Rev. B* 100, 125124 (2019).
- [22] Taco Cohen and Max Welling. Group equivariant convolutional networks. In *International conference on machine learning*, pages 2990–2999. PMLR, 2016.
- [23] C. Roth and A. H. MacDonald, Group Convolutional Neural Networks Improve Quantum State Accuracy, arXiv:2104.05085
- [24] Moshir Harsh, Jérôme Tubiana, Simona Cocco and Rémi Monasson, 'Place-cell' emergence and learning of invariant data with restricted Boltzmann machines: breaking and dynamical restoration of continuous symmetries in the weight space, *J. Phys. A: Math. Theor.* 53 174002 (2020).

- [25] Alessandro Ingrosso, Sebastian Goldt, Data-driven emergence of convolutional structure in neural networks, *Proc. Natl. Acad. Sci. U.S.A.* 119, e2201854119 (2022).
- [26] Michael Y. Pei and Stephen R. Clark, Compact neural-network quantum state representations of Jastrow and stabilizer states, *J. Phys. A: Math. Theor.* 54, 405304 (2021)
- [27] Torlai, G. et al. Neural-network quantum state tomography. *Nat. Phys.* 14, 447–450 (2018).
- [28] E. Fedotova, N. Kuznetsov, E. Tiunov, A.E. Ulanov, and A.I. Lvovsky, Continuous-variable quantum tomography of high-amplitude states, *Phys. Rev. A* 108, 042430 (2023)
- [29] E. S. Tiunov, V. V. Tiunova (Vyborova), A. E. Ulanov, A. I. Lvovsky and A. K. Fedorov, Experimental quantum homodyne tomography via machine learning, *Optica* 7, 448 (2020).
- [30] R. H. Dicke, Coherence in Spontaneous Radiation Processes, *Physical Review* 93(1), 99 (1954)
- [31] Davide Girolami, Tommaso Tufarelli, and Cristian E. Susa, Quantifying Genuine Multipartite Correlations and their Pattern Complexity, *PRL* 119, 140505 (2017).
- [32] H.D. Ursell, “The evaluation of Gibbs’ phase-integral for imperfect gases,” in *Mathematical Proceedings of the Cambridge Philosophical Society*, Vol. 23 (Cambridge University Press, 1927) pp. 685–697.
- [33] H. J. Lipkin, N. Meshkov, and A. J. Glick, Validity of many-body approximation methods for a solvable model: (I). Exact solutions and perturbation theory, *Nucl. Phys.* 62, 188 (1965).
- [34] N. Meshkov, A. J. Glick, and H. J. Lipkin, Validity of many-body approximation methods for a solvable model: (II). Linearization procedures, *Nucl. Phys.* 62, 199 (1965).
- [35] A. J. Glick, H. J. Lipkin, and N. Meshkov, Validity of many-body approximation methods for a solvable model: (III). Diagram summations, *Nucl. Phys.* 62, 211 (1965).
- [36] Yusuke Nomura, Investigating Network Parameters in Neural-Network Quantum States, *Journal of the Physical Society of Japan* 91, 054709 (2022)
- [37] Kenny Choo, Giuseppe Carleo, Nicolas Regnault, and Titus Neupert, Symmetries and Many-Body Excitations with Neural-Network Quantum States, *Phys. Rev. Lett.* 121, 167204 (2018).
- [38] Mohamed Hibat-Allah, Roger G. Melko, and Juan Carrasquilla, Investigating topological order using recurrent neural networks, *Phys. Rev. B* 108, 075152 (2023)
- [39] Mohamed Hibat-Allah, Martin Ganahl, Lauren E. Hayward, Roger G. Melko, and Juan Carrasquilla, Recurrent neural network wave functions, *Phys. Rev. Research* 2, 023358 (2020)
- [40] Luciano Loris Viteritti, Riccardo Rende, and Federico Becca, Transformer Variational Wave Functions for Frustrated Quantum Spin Systems, *Phys. Rev. Lett.* 130, 236401 (2023).
- [41] Luciano Loris Viteritti, Riccardo Rende, Alberto Parola, Sebastian Goldt, Federico Becca, Transformer Wave Function for the Shastry-Sutherland Model: emergence of a Spin-Liquid Phase, arXiv:2311.16889
- [42] <https://github.com/PIQuIL/QuCumber>
- [43] Shun-ichi Amari, *Information Geometry and Its Applications* (Springer Japan 2016).
- [44] Giacomo Torlai, *Augmenting Quantum Mechanics with Artificial Intelligence*, Thesis, Waterloo, Ontario, Canada, 2018
- [45] Giuseppe Carleo, Yusuke Nomura and Masatoshi Imada, Constructing exact representations of quantum many-body systems with deep neural networks, *Nature Communications* 9, 5322 (2018).
- [46] Xun Gao and Lu-Ming Duan, Efficient representation of quantum many-body states with deep neural networks, *Nature Communications* 8, 662 (2017)
- [47] Ivan Glasser, Nicola Pancotti, Moritz August, Ivan D. Rodriguez, and J. Ignacio Cirac, Neural-Network Quantum States, String-Bond States, and Chiral Topological States, *PRX* 8, 011006 (2018)
- [48] Stephen R. Clark, Unifying Neural-network Quantum States and Correlator Product States via Tensor Networks, *J. Phys. A: Math. Theor.* 51 135301 (2018).
- [49] M. G. M. Moreno, Fernando Parisio, All bipartitions of arbitrary Dicke states, arXiv:1801.00762
- [50] Wang, X.; Girshick, R.; Gupta, A.; and He, K. 2018. Non-local neural networks. In *Proceedings of the IEEE conference on computer vision and pattern recognition*, 7794–7803
- [51] Vaswani, A.; Shazeer, N.; Parmar, N.; Uszkoreit, J.; Jones, L.; Gomez, A. N.; Kaiser, Ł.; and Polosukhin, I. 2017. Attention is all you need. *Advances in neural information processing systems*, 30.
- [52] Dong-Ling Deng, Xiaopeng Li, and S. Das Sarma, Quantum entanglement in neural network states, *Phys. Rev. X* 7, 021021 (2017)
- [53] F. Verstraete, M. Popp, and J. Cirac, Entanglement versus correlations in spin systems. *Phys. Rev. Lett.* 92, 027901 (2004)
- [54] Konstantin V. Krutitsky, Andreas Osterloh and Ralf Schützhold, Avalanche of entanglement and correlations at quantum phase transitions, *Sci.Rep.* 7, 3634 (2017).